The 2013 World Congress on
Advances in Structural Engineering and Mechanics (ASEM13)
Jeju, Korea, September 8-12, 2013

Analytical Tension Stiffening Model of Inoxydable Steel in Comparison with Carbon Steel

S. Alih[2)], *A. Khelil[1)], H. Fares[2)],

[1),] Lorraine University, IJL UMR 7198 CNRS, Equipe 207, IUT Nancy Brabois CS 90137, F54601 Villers Les Nancy, France
[2)]Faculty of Civil Engineering, Universiti Teknologi Malaysia, 81310 Johor Bahru, Johor Malaysia

[1)] abdel.khelil@univ-lorraine.fr

ABSTRACT

This paper presents the interaction properties between inoxydable steel and concrete. A tension stiffening model is develop to define the interaction behavior. This model is integrated in the global analysis of a composite concrete beam reinforced with inoxydable steel. An inverse method based on the combination of experimental and numerical results obtained from a nonlinear analysis (NNA) is developed to determine the model parameters. The tension stiffening model developed for inoxydable steel is compared with standard carbon steel. Results obtained show that the stiffening effect of concrete with inoxydable steel is higher during the cracking phase in comparison to the standard steel.

1. INTRODUCTION

Concrete is a material of low tensile strength, cracking of reinforced concrete structures generally occur for low service charges. In a bent section, the mechanical contribution of the concrete is often overlooked for standard concrete. The design rules and analysis of existing structures do not take into account the mechanical contribution of concrete in tension. In the overall analysis of a composite concrete element, the behavior of a steel bar alone is not the same as that of a bar embedded in concrete. The grip allows the concrete between cracks to resist tensile forces, thereby reducing the average level of stress in the steel. This results in a gain of rigidity; called the

[2)] Assistant professor
[1)] Professor

tension stiffening effect [3]. In global behavior, this effect allows to take into account the positive contribution of the concrete surrounding the bars.

A simple way to consider this local phenomenon is to use an average stress-strain curve of concrete in tension in the global analysis (Ying-Wu Zhou and Yu-Fei Wu, 2011). Several investigations have been developed to model this phenomenon in order to predict the behavior of structures by changing the laws of behavior of one of the two materials in the presence (this hardening can be incorporated into one or other of the laws of behavior of steel and concrete materials). For concrete this effect is included by adding, after cracking and when analyzing the global behavior of the element, a descending branch to the constitutive law of concrete in tension. For this study, we adapted the behavioral model proposed by Rim Nayal and Hayder A. Rasheed, (2006) (Figure 1) to represent the properties of interaction between the stainless steel reinforcement and concrete. Four parameters Cd, Cb, Cp, and Cs are needed to fully characterize this model. The mechanical properties of concrete in the traction phase are $f'_{t,}$ and ε_{cr}.

Parameters involved in defining the interaction properties between concrete and Inoxydable steel as reinforcing bars in structural element are determined through an inverse approach combining results from laboratory and NNA. Since tension stiffening models are adopted by smeared crack approach to simulate global response, the present approach rationally develops those parameters through direct matching of detailed nonlinear beam analysis and experimental global response. By comparing the load-deflection values obtained from the NNA with the results from laboratory test, tension stiffening model is chosen based on the closest resemblance between results from these two methods.

Tension stiffening model as been suggested by Nayal and Rasheed, 2006 is chosen to represent the interaction properties between inoxydable steel and concrete. This model has only a single set of stiffening parameters which applicable to the entire tension zone at all steps of analysis. Due to its simplicity and ability to simulate the post-cracking behavior, this model is used further in this study. Fig. 3.26 shows the tension stiffening model, which depicts the main phenomena of primary and secondary cracking. This model involved four parameters; C_d, C_b, C_p, C_s together with the character of concrete; f'_t and ε_{cr} where

$$f'_t = 0.3 f_{ck}^{\left(\frac{2}{3}\right)} \quad (1)$$

$$\varepsilon_{cr} = \frac{f'_t}{E} \quad (2)$$

These concrete characters are determined based on a compression test conducted on the concrete sample used to prepare the concrete beam. These properties are discussed in Section 3.3.1. The four parameters are the one need to be determined through the inverse approach combining results from laboratory and NNA. Detail procedures are discussed in the following sub-sections.

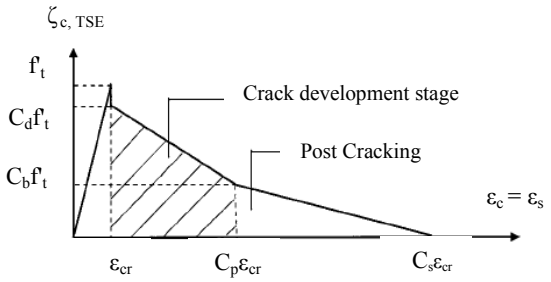

Fig. 1. Tension stiffening model used to represent interaction properties between Inoxydable steel and composite concrete.

2. INVERSED METHOD APPROACH

In order to determine the four parameters in the tension stiffening model, NNA is conducted on the beam section to determine the load-deflection curve based on the section and beam properties. Laboratory sample of the concrete beam reinforced with austenitic-hot and the bending test results are used in this analysis. This analysis consist of two main stages; i) section analysis, ii) beam analysis. Beam properties shown in Fig. 3.14 are used in the section analysis and results of the laboratory test is used in the beam analysis phase. To analyze the beam section properties, cross-section of the beam is divided vertically into small layers through its total height as shown in Fig. 3.30. It is divided into 28 layers in which each layer is 10mm height. Compression and tension zones of the section are identified, and strain at the center of each layer is then computed. Stress in each layer is evaluated using the corresponding material model. For beam analysis, beam is divided horizontally into small sections as shown in Fig. 3.33. Beam is divided into 295 sections along its total length in which each section is 10mm long.

Fig. 3.27 shows the steps taken in conducting the NNA. In the beginning of the analysis, initial values of the tension stiffening parameters are introduced to the program together with the other properties of the RC beam obtained from laboratory samples. These include the materials and geometrical properties.

In the first iteration, section analysis will provide the properties detail for a particular section of the beam for each load increment. These properties will then be used in the beam analysis in order to determine load-deflection curve at mid-span of the beam. The load-deflection curve obtained from this NNA is then compared with the one obtained from laboratory work; bending test on the beam sample. The tension stiffening model applied in the section analysis is then corrected by changing the values of the four parameters; C_d, C_b, C_p, C_s so the load-deflection curve values from NNA resemble well with the laboratory results. The set of parameters which give the best-fit values with laboratory is selected as the tension stiffening model to represent the concrete beam reinforced with Inoxydable steel bars. These inversely estimated values give more reliable representation of interaction properties between the inox and composite concrete. This concept is visualized in Fig. 3.28.

If the coefficient of determination, R^2 between the two curves is more than 0.9, the values set of C_d, C_b, C_p, C_s will be chosen as the tension stiffening parameters for

Inoxydable steel. Otherwise, second iteration will be conducted with a new set of parameters and the whole process will be repeated all over again.

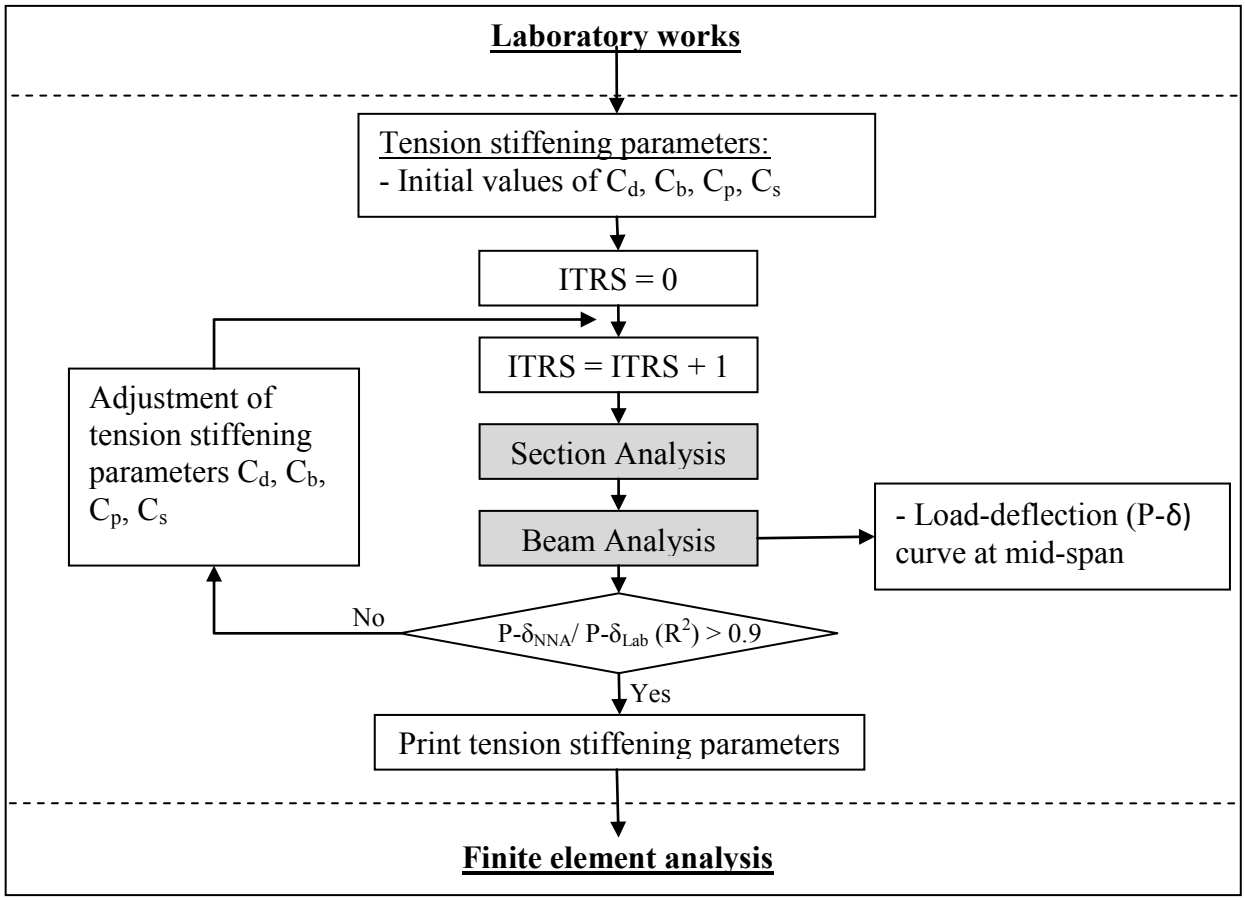

Fig. 2. Steps in the nonlinear numerical analysis

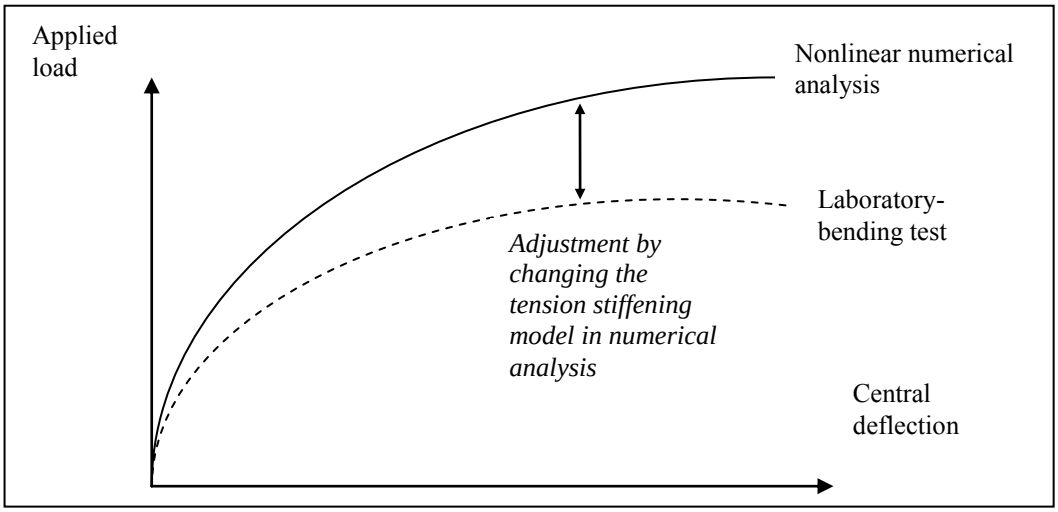

Fig. 3. The tension stiffening model is inversely develop by changing the parameters value used in section analysis so the central deflection obtained through NNA resemble the real laboratory results.

2. 1 Material Models

For concrete layers in compression zones, a fourth-degree polynomial model is chosen to represent the stress-strain relation;

$$\sigma_c = a_0 + a_1\varepsilon_c + a_2{\varepsilon_c}^2 + a_3{\varepsilon_c}^3 + a_4{\varepsilon_c}^4 \quad (3)$$

The above polynomials have been proposed on the basis of agreement with experimental work. They, moreover have distinct advantage of being directly differentiable and integrable. The coefficients in Eq. 3.23 are defined by using the curve boundary condition based on concrete properties shown in Fig. 3.29;

$$\begin{Bmatrix} a_0 \\ a_1 \\ a_2 \\ a_3 \\ a_4 \end{Bmatrix} = \begin{bmatrix} 1 & 0 & 0 & 0 & 0 \\ 0 & 1 & 0 & 0 & 0 \\ 1 & \varepsilon_m & \varepsilon_m^2 & \varepsilon_m^3 & \varepsilon_m^4 \\ 0 & 1 & 2\varepsilon_m & 3\varepsilon_m^2 & 4\varepsilon_m^3 \\ 1 & 1 & 2C_u\varepsilon_m & 3(C_u\varepsilon_m)^2 & 4(C_u\varepsilon_m)^3 \end{bmatrix}^{-1} \begin{Bmatrix} 0 \\ E_{ci} \\ f_m \\ 0 \\ E_{cf} \end{Bmatrix} \quad (4)$$

where

$$f_m = k_c.f_c^{'} \quad (5)$$

k_c = 0.85, 1.0 or > 1.0 according to some investigators. In this study k_c is taken as 1.0. As shown in Fig. 3.30, the slope of the descending line is evaluated by expressions suggested by Kent and Park (2006) to include the effect of hoop confinement. The relation is extended horizontally when a stress of $0.2f_m$ is reached and it is terminated at a maximum confined compressive strain $C_c\epsilon_m$.

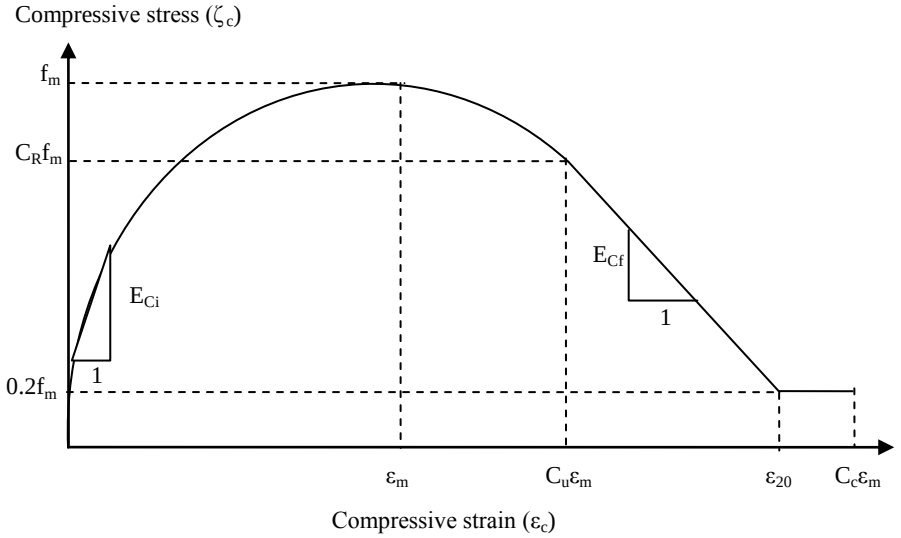

Fig. 4. Stress-strain relation for compressive concrete used in the analysis

For concrete in tension zone, the stress-strain relation of reinforced concrete suggested by Gilbert and Warner (2006) (Fig. 2.7) is adopted to represent the tensile behavior combining tension softening, tension stiffening and local bond-slip effects. This relation is well backed by experimental curve of plain concrete and compared well with test results on reinforced concrete slab conducted by the same authors.

Furthermore it is well suited to the present method of analysis. However in this study, the softening parameters are not changed according to the fibre location relative to the steel position, in which tension softening is ignored, but rather a continuous function is adopted over the whole tension zone. Fig. 3.26 shows the concrete stress-strain relation in tension used in the analysis. The four parameters C_d, C_b, C_p, and C_s are set to an initial trial values at the beginning of the analysis and inversely estimated from a combination of nonlinear analysis and experimental results.

For reinforcement bars, a bilinear relation is considered adequate for proper simulation of the actual stress-strain relation for reinforcing steel used in compression zone (carbon steel Grade 460) since the elastic-plastic behavior with or without introducing the strain hardening effect is easily simulated by controlling the slope of the second line. However, for tension zone where Inoxydable steel bars are used, a specific constitutive law developed in Section 3.2.3 (Eq. 3.17 and 3.18) is applied to represent the nonlinearity of this type of steel.

2. 2 Section Analysis

Increasing the loading (axial force and/or bending moment) applied to a section, causes the neutral axis depth, the strain and stress distributions, and the flexural and axial rigidities to vary in a nonlinear manner. Numbers of studies involving numerical techniques have therefore been conducted to tackle this situation. Bilinear and trilinear moment-curvature relations for flexural members are example of early and simple models. However, such models are incapable of tracing an accurate response for heavily reinforced sections, especially in presence of an axial force (Garion, C., Skoczen´, B., and Sgobba, S. (2006)). In this study, a nonlinear solution scheme is utilized within which direct and exact computations are made by performing closed-form integrations for nonlinear section properties. The section analysis involved determination of overall effective or secant flexural rigidity (EIs) for the beam section. The strain profile is determined using the applied moment and the current value of the EIs about the inelastic centroid. The compression and tension zones of the section are identified. For each layer, strain is computed to evaluate the stress using the corresponding material model.

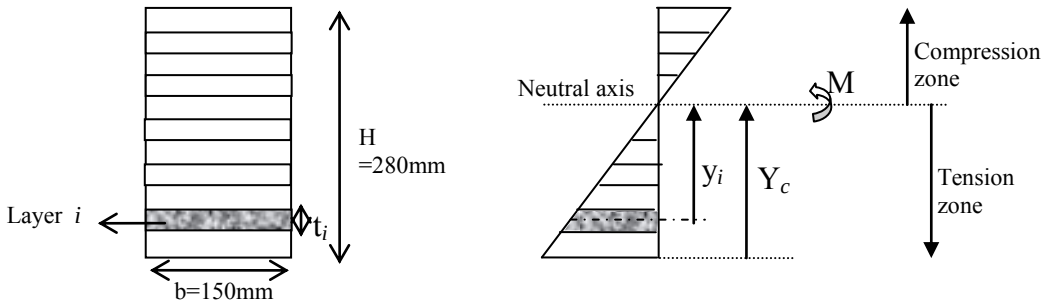

Fig. 5. Section analysis by finite layer approach

The overall effective or secant axial rigidity of the section (EA_s) is the summation of the individual layer areas times their corresponding secant modulus of elasticity:

$$EA_s = \sum_{i=1}^{NLR} E_{ci} B_{ci} t_{ci} + \sum_{j=1}^{N} \left(E_{rtj} - E_{ctj}\right) A_{rtj} + \sum_{k=1}^{M} (E_{rbk} - E_{cbk}) A_{rbk} \quad (6)$$

$$E_{ci} = \frac{\sigma_{ci}}{\varepsilon_{ci}} \quad (7)$$

$$E_{rtj} = \frac{\sigma_{rtj}}{\varepsilon_{rtj}} \quad (8)$$

$$E_{rbk} = \frac{\sigma_{rbk}}{\varepsilon_{rbk}} \quad (9)$$

Where

NLR = number of concrete layers in the section

N, *M* = numbers of the top and bottom reinforcement layers, respectively

E_{ci} = secant concrete modulus

B_{ci} = width of layer *i*

t_{ci} = thickness of layer *i*

E_{rtj} and E_{rbk}= secant moduli of elasticity of the top and bottom reinforcement layers

A_{rtj} and A_{rbk}= corresponding reinforcement areas

E_{ctj} and E_{cbk}= secant concrete moduli of elasticity at the level of the top and bottom reinforcement layers respectively

ε_{ci} , ε_{rtj} and ε_{rbk}= strain at the center of concrete layer *i*, top and bottom reinforcement layer *j* and *k* respectively

σ_{ci} , σ_{rtj} and σ_{rbk}= stress at the center of concrete layer *i*, top and bottom reinforcement layer *j* and *k* respectively corresponding to material models

The overall effective or secant flexural rigidity (EI_s) of the section is the flexural rigidity of each layer about the inelastic centroid (Y_c) summed up over the section depth. The inelastic centroid being the position about which the first moment of the axial rigidity (*EA*) vanishes (Fig. 3.30).

$$EI_s = \sum_{i=1}^{NLR} E_{ci} B_{ci} t_{ci} Y_i^2 + \sum_{j=1}^{N} \left(E_{rtj} - E_{ctj}\right) A_{rtj} \left(Y_{rtj}\right)^2 + \sum_{k=1}^{M} (E_{rbk} - E_{cbk}) A_{rbk} (Y_{rbk})^2 \quad (10)$$

where

Y_i= distance from the centroid of layer *i* to the section inelastic centroid

Y_{rtj} and Y_{rbk} = distance from the inelastic centroid to the centroid of the top and bottom reinforcement layers respectively.

The internal axial force (F_x) is given by;

$$F_s = \sum_{i=1}^{NLR} E_{ci} \varepsilon_{ci} B_{ci} t_{ci} + \sum_{j=1}^{N} \left(E_{rtj} - E_{ctj}\right) \varepsilon_{rtj} A_{rtj} + \sum_{k=1}^{M} (E_{rbk} - E_{cbk}) \varepsilon_{rbk} A_{rbk} \quad (11)$$

The internal bending moment (M_{int}) about the inelastic centroid is represented by;

$$M_{int} = \sum_{i=1}^{NLR} E_{ci} \varepsilon_{ci} B_{ci} t_{ci} Y_i + \sum_{j=1}^{N} \left(E_{rtj} - E_{ctj}\right) \varepsilon_{rtj} A_{rtj} \left(Y_{rtj}\right) + \sum_{k=1}^{M} (E_{rbk} - E_{cbk}) \varepsilon_{rbk} A_{rbk} (Y_{rbk}) \quad (12)$$

To develop an approach which lends itself to direct computation, the section is divided into two zones each of which is bounded by one of the extreme fibers and the neutral axis. According to the type of stress in any zone (tension or compression), it is further divided into regions having a certain stress-strain formula for each. The compression zone may include one or more of the following regions (Fig. 3.29):

Concrete:	Region 1	$0 \leq \varepsilon_c \leq C_u \varepsilon_m$
	Region 2	$C_u \varepsilon_m < \varepsilon_c \leq \varepsilon_{20}$
	Region 3	$\varepsilon_{20} < \varepsilon_c \leq C_u \varepsilon_m$
Steel:	Region 4	$0 \leq \varepsilon_{sc} \leq \varepsilon_y$
	Region 5	$\varepsilon_y \leq \varepsilon_{sc} \leq \varepsilon_{su}$

The tension zone may also include one or more of the following regions:

Concrete:	Region 1	$-\varepsilon_{cr} \leq \varepsilon_t \leq 0$
	Region 2	$-C_p \varepsilon_{cr} \leq \varepsilon_t \leq -\varepsilon_{cr}$
	Region 3	$-C_s \varepsilon_{cr} \leq \varepsilon_t \leq -C_p \varepsilon_{cr}$
Steel:	Region 4	$-\varepsilon_y \leq \varepsilon_{st} \leq 0$
	Region 5	$-\varepsilon_{su} \leq \varepsilon_{st} \leq -\varepsilon_y$

Explicit forms of the rigidities and the internal loadings for all the regions are derived by performing analytical integrations, as detailed in the following sub-section. By the summation of the region properties, the section properties are directly obtained.

$$EA_s = \sum_{i=1}^{2} \sum_{j=1}^{NRi} EA_{ij} \quad (13)$$

$$F_x = \sum_{i=1}^{2} \sum_{j=1}^{NRi} F_{x_{ij}} \quad (14)$$

$$EI_s = \sum_{i=1}^{2} \sum_{j=1}^{NRi} EI_{ij} \quad (15)$$

$$M_{int} = \sum_{i=1}^{2} \sum_{j=1}^{NRi} M_{c_{ij}} \quad (16)$$

where NRi is the number of regions per zone. The above equations; Eq. (3.33)-(3.36) are detailed in Annex 7.1.

The effective section properties corresponding to any applied bending moment step, M, are evaluated as follows:

1. The instantaneous curvature is determined by dividing the applied moment by the most current value of the effective section flexural rigidity:

$$\phi = \frac{M}{EI_s} \quad (17)$$

2. The depth of the tension and the compression zones are defined using the most recent location of the inelastic centroid Y_c and the total height of the section H:

$$Y_{N1} = H - Y_c \quad (18)$$

$$Y_{N2} = Y_c \quad (19)$$

3. The section rigidities (EA_s, EI_s), internal axial force (F_x), and the bending moment (M_{int}) are calculated for the present strain distribution using Eqs. (3.26), (3.30)-(3.32).

4. The accuracy of the most recent inelastic centroid position is investigated using the criterion of vanishing the moment of axial rigidity about the current centroid (*ES*) at the correct position:

$$ES = \frac{F_x}{\phi} \tag{20}$$

A normalized convergence criterion is adopted with a certain tolerance limit depending on the level of accuracy required.

$$\frac{ES}{EA_s x Y_c} < S_{TOL} \Longrightarrow Convergence\ achieved \tag{21}$$

Where S_{TOL} is the convergence tolerance of the section; taken as $5x10^{-7}$.

5. If Eq. (3.41) is satisfied, an equilibrium solution is reached, yielding the inelastic centroid position and the section properties for that step. Otherwise, steps 1-4 are repeated using the corrected inelastic centroid Y_c until convergence is achieved:

$$Y_{c(corrected)} = Y_{c(current)} + \frac{ES}{EA_s} \tag{22}$$

6. The analysis is stopped when a failure criterion is satisfied (F_{CON}). The failure criteria implemented are rupture of reinforcement or crushing of concrete. Concrete crushing failure is defined at 0.003 compressive strain for unconfined compression and a higher value for confined concrete (the strain at which the compression stress of the descending branch reaches 0.2 f_c). Rupture failure occurs when the reinforcement reaches the ultimate rupture strain.

The above procedures are programmed using MATLAB to automate the section analysis for each load increment. Fig. 3.32 shows the flow chart of the program.

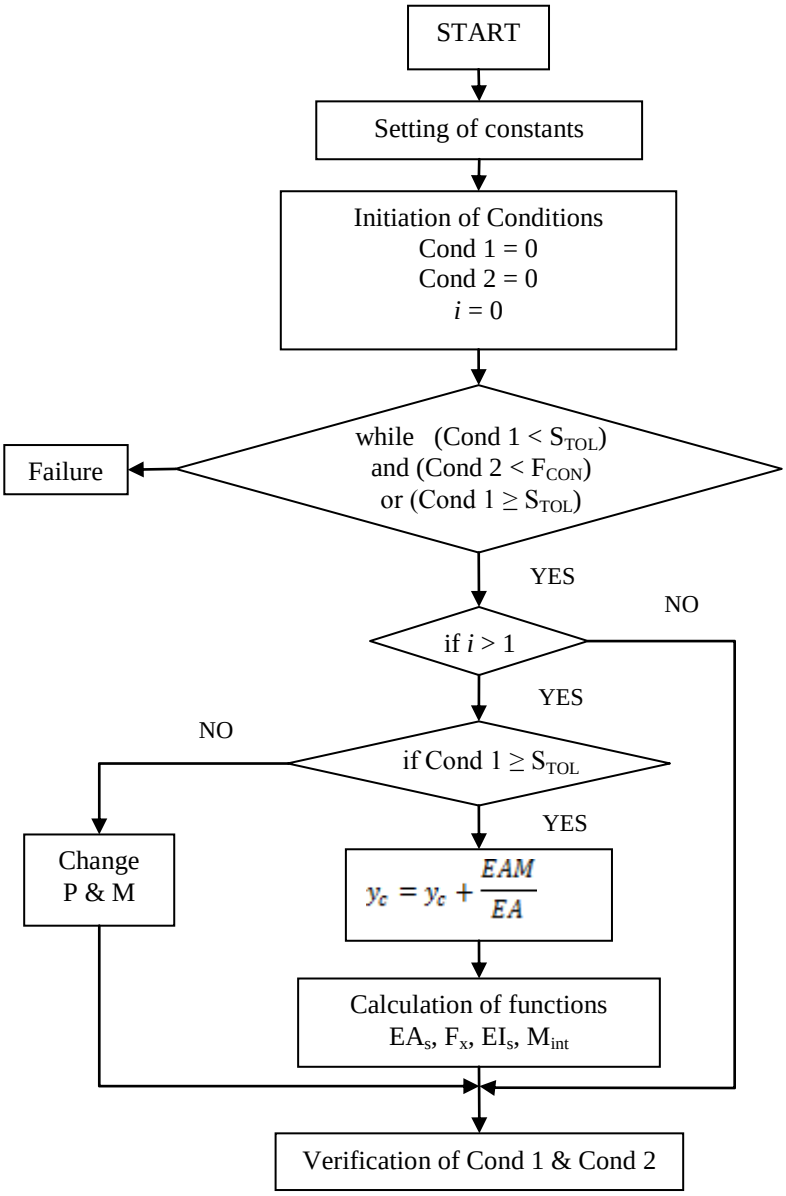

Fig. 6. Flow chart of the nonlinear numerical analysis programmed using MATLAB

2. 3 Beam Analysis

The nonlinear load-deflection solution of the beam is formulated using the moment area integration. Because the flexural rigidity reduces with an increase in moment, the stiffness of the beam is expected to vary along the span, in a nonlinear fashion, with the change in bending moment. This study is intended to consider an accurate stiffness distribution along the beam. This is accomplished by dividing the beam into a large number of segments and calculating the section flexural rigidity in the middle of each segment under a certain load increment. The beam sample is divided into 295 segments; 10mm width for each segment (Fig. 3.33). The mid-span deflection, in symmetrically loaded simple beams, is obtained by performing numerical integration

of the moment of curvature distribution along half the span about the support point. The numerical integration is performed as a summation of the analytical integration contribution of each segment. This is expressed for the four-point bending case as

$$\Delta_{midspan} = \int_0^{L/2} x\varphi(x)dx \tag{23}$$

$$= \sum_{i=1}^{N_s} \frac{P}{2EI_{si}} \left[\frac{X_{i+0.5}^3 - X_{i-0.5}^3}{3}\right] + \frac{PL_a}{2EI_{si}} \frac{\left[\left(\frac{L}{2}\right)^2 - (L_a)^2\right]}{2} \tag{24}$$

where N_s=number of segments along the beam shear span; P=total load applied on the beam; $X_{i-0.5}$=distance from the support point to the beginning of segment i; $X_{i+0.5}$=distance from the support point to the end of the segment i; L_a=shear span of the beam, and EI_{si}=flexural rigidity of segment i (Fig. 3.34).

The mid-span deflection is then plotted and compared to the curve obtained from laboratory test, as illustrated in Fig. 3.28. The tension stiffening model applied in the section analysis is then corrected by changing the values of the four parameters; C_d, C_b, C_p, C_s so the load-deflection curve values from NNA resemble well with the laboratory results. The set of parameters which give the best-fit values with laboratory is selected as the tension stiffening model to represent the concrete beam reinforced with Inoxydable steel bars. These inversely estimated values give more reliable representation of interaction properties between the inox and composite concrete.

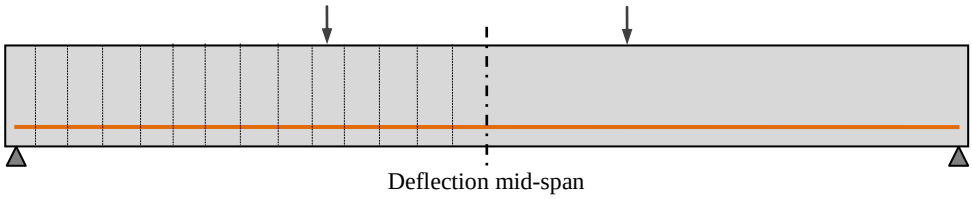

Fig. 7. Numerical analysis: Beam is divided into a large number of sections to determine the central deflection. Each section is analyzed to get stress, strain, and section rigidities for every increment of load

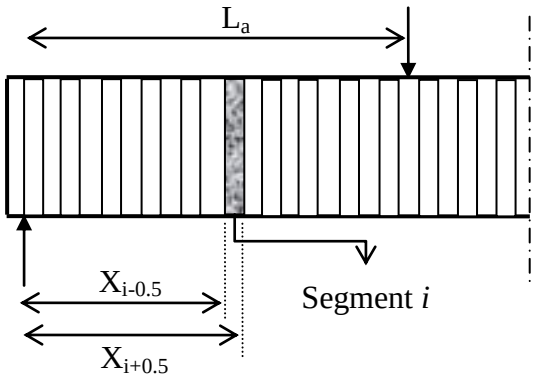

Fig. 8. Vertical segment of the beam analysis

3. TENSION STIFFENING MODEL FOR INOXYDABLE STEEL

Results obtained from the NNA are compared with laboratory findings in order to determine the tension stiffening model for inox. The beam sample constructed and tested under bending as been discussed in Section 3.5.1 is used in the analysis. Mechanical and geometrical properties of the beam are applied as input to the program.

A series of analyses are conducted to determine the tension stiffening parameters that correlate well with the real behavior of the RC beam as per laboratory findings. Table 3.3 shows the four sets of trial on selecting the values of C_d, C_b, C_p, C_s. Based on the section properties obtained from NNA, and load-deflection values from beam analysis, comparison with laboratory results gives value of 0.9, 0.5, 5 and 13 for C_d, C_b, C_p, C_s respectively. The load-deflection curve from NNA using these tension stiffening parameters are compared with laboratory curve in Fig. 3.35. Good correlation can be observed from these two curves. Fig. 3.36 shows the final tension stiffening model develop for composite concrete beam reinforced with inoxydable steel from austenitic type. This model is useful to represent the interaction behavior between these two materials in any finite element modeling works.

Table 1. Investigation of tension stiffening parameters

Parameter	Selecting C_d	Selecting C_b	Selecting C_p	Selecting C_s	Selected parameters
C_d	0.8,**0.9**,1	1.5	1.5	1.5	0.9
C_b	0.5	0.45, **0.5**, 1	0.8	0.8	0.5
C_p	4	4	4, **5**, 6	4	5
C_s	40	40	40	5, 10, **13**, 20	13

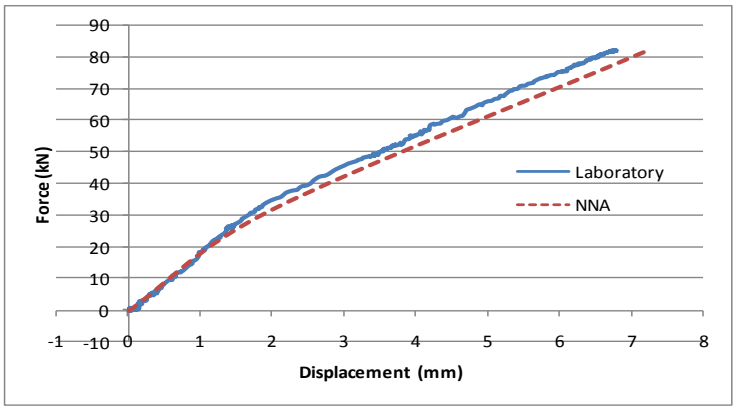

Fig. 9. Force displacement curve from laboratory results compared to the nonlinear numerical analysis

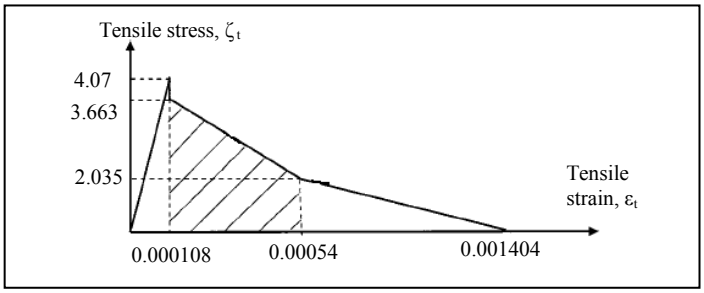

Fig. 10. Tension stiffening model for beam reinforced with inoxydable steel bars

4. COMPARISON WITH CARBON STEEL

According to a study conducted by Nayal and Rasheed (2006), selected values for tension stiffening parameters for concrete beam reinforced with carbon steel are 0.8, 0.45, 4, and 10 for Cd, Cb, Cp, and Cs respectively. Fig. 3.37 shows the tension stiffening model for inoxydable steel as compared to the standard carbon steel.

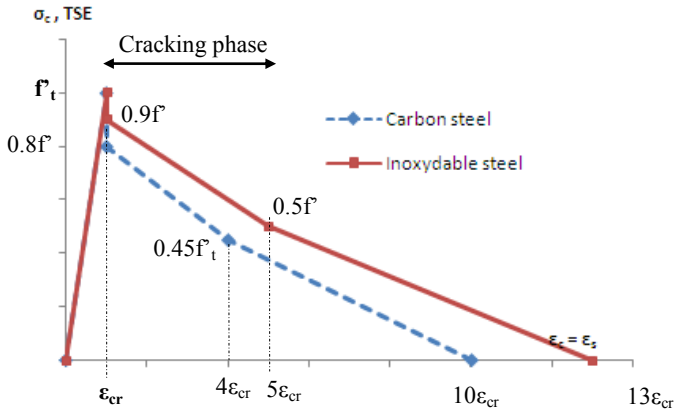

Fig. 11. Comparison of tension stiffening model for concrete beam reinforced with carbon steel and inoxydable steel

Referring to Fig. 3.37. it can be observed that concrete beam reinforced with inoxydable steel has higher tension stiffening effect than the one reinforced with standard carbon steel. In the cracking phase, the tension stiffening with inoxydable steel increases 50 percent as compared to standard steel.

Approach suggested in this study is able to determine parameters involved in developing the tension stiffening model. Based on the inverse method, a more reliable result could be generated. This tension stiffening model could be used further in any numerical simulation to represent the interaction properties between inoxydable steel and concrete in composite material.

5. CONCLUSION

In this approach, the grip that allows concrete between cracks to resist tensile forces in composite concrete is investigated using an inverse approach which combines results from the experimental works with a nonlinear numerical analysis. Constitutive law for inox developed in an earlier study by the authors Alih and Khelil (2012) is integrated into the nonlinear numerical analysis of reinforced concrete elements based on discretization in horizontal layers for the analysis section and a vertical discretization for the overall analysis. The parameters are identified inversely by comparing experimental results and those from the numerical calculation. Comparison between experimental results and the prediction of the numerical analysis shows a very good correlation.

REFERENCES

Ying-Wu Zhou and Yu-Fei Wu, (2011) General model for constitutive relationships of concrete and its composite structures, *Composite Structures*; 08(022): 1-13.

Rim Nayal and Hayder A. Rasheed, (2006) Tension stiffening model for concrete beams reinforced with steel and FRP bars, *Journal of Materials in Civil Engineering*; 18(6): 831-841.

Yuichi Sato and Frank J. Vecchio,(2003) Tension stiffening and crack formation in reinforced concrete members with fiber-reinforced polymer sheets, *Journal of Structural Engineering*; 129 (6): 717-724.

Abdelhafid Bouzaiene and Bruno Massicotte, (1997) Hypoelastic tridimensional model for nonproportional loading of plain concrete, *Journal of Engineering Mechanics;:* 123(11): 1111-1119.

EN 1992-1-1. Eurocode 2 – (2003). Design of concrete structures, Part 1.1, General rules and rules for buildings.

Garion, C., Skoczen´, B., and Sgobba, S. (2006). Constitutive Modelling and Identification of Parameters of the Plastic Strain-Induced Martensitic Transformation in 316L Stainless Steel at Cryogenic Temperatures. *International Journal of Plasticity*. Vol. 22, 1234–1264.

S. Alih, A. Khelil, (2011), Behavior of Inoxydable Steel and their Performance as Reinforcement Bars in Concrete Beam: Experimental and Nonlinear Finite Element Analysis, *Construction and Building Materials*, 37, 481-492.